Articles

Initial Capacity Fading of Meso-phase Pitch Based Carbon Fiber as Anode Material of Lithium Ion Battery

Chil-Hoon Doh,* Seong-In Moon, Mun-Soo Yun, and Duk-Hyung Yum†

Battery Research Group, Korea Electrotechnology Research Institute, Changwon 641-120, Korea
†Battery R&D Center, STC Corporation, Kumi 730-030, Korea
Received August 4, 1998

The origin of initial capacity fading of MPCF3000, an artificial graphite fiber, as anode material for lithium ion batteries was studied with organic electrolytic solution 1M $LiPF_6$ in ethylene carbonate (EC) and diethyl carbonate (DEC) (1 : 1). There was a reversible potential plateau at the region of 30 ~ 60 mV_{Li/Li^+}. This potential plateau disappeared during cycling, leading to fast capacity fading and low Ah efficiency. This potential plateau was not influenced by the charging to 50 mV_{Li/Li^+}. When the electrode was charged by constant current step pulse (20 charges to 22.7 mA/g-carbon with each charge followed by 30 minutesof rest, and another 20 charges to 3.78 mA/g-carbon with each charge followed by 30 minutes of rest) to the potential of 5 mV_{Li/Li^+}, the plateau was found at the first cycle only.

Introduction

The carbon material used for the anode of a lithium ion battery should undergo minimum structural change during lithium intercalation, no irreversible reaction with the electrolytic solution and no trapping[1] of lithium in the carbon structure. Characteristics of carbon materials vary by their morphology and crystal structure.[2] The latter can be described by the in-plane cell constant (d_{100}), inter-layer spacing (d_{002}), coherence length in the AB plane (La), longitudinal length in the c-axis (Lc), probability of random stacking (Pr), probability of translation (Pt), and degree of graphitization (g) based on physical meaning.[3,4] The crystal structure of carbon is closely related to heat treatment temperature (HTT). Generally, an increase in HTT leads to an increase in g, La and Lc, and to a decrease in Pr and Pt.[5] Variations in the pattern of structural parameters are related to the carbon precursor material and processing history. Graphitic material display staging phenomena during intercalation of lithium ion[6~8] that show distinguishable potential differences among stages.

Artificial graphite such as graphitized meso-phase carbon micro-bead (g-MCMB)[9,10] does not have a potential plateau between 0-50 mV_{Li/Li^+} as open circuit potential (OCP)[11] in general. Such a region of potential plateau appears in low temperature heat treated carbon,[12~15] including soft carbon and hard carbon. Yamabe *et al.*[16] performed molecular orbital (MO) calculations of low potential charging to propose an adsorption model rather than an intercalation model. Adsorbed lithium clusters on graphite layer comprised 2-10 atoms based on MO calculations. Such clusters have a cationic property interacting electron rich π cloud of graphite layer. This is also supported by other publications.[17,18] Graphitized meso-phase pitch based carbon fiber (MPCF)[19,20] has a potential plateau between 0-50 mV_{Li/Li^+} as OCP in spite of the use of artificial graphite carbon.

We tried to verify characteristics of the potential plateau that disappeared during the charge-discharge process by evaluating the initial capacity fading property. Three methods were used to determine initial capacity fading characteristics, employing the following preliminary charge-discharge

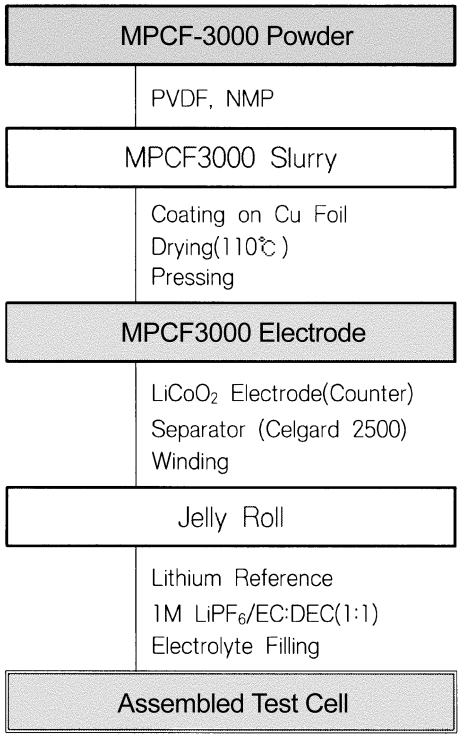

Scheme 1

*To whom correspondence should be addressed. Tel: 0551-280-1662, Fax: 0551-280-1606, E-mail: chdoh@keri.re.kr

conditions. The first method involved cycling of the galvanostatic charge-discharge between 50 mV and 1500 mV_{Li/Li^+} ten times. The second and the third methods involved the prolonged first charging at a potential of 50 mV and 5 mV_{Li/Li^+}, alternately, using the galvanostatic charge-rest method.

Experimental Section

XRD & SEM Analyses. MPCF was manufactured by Petoca, Ltd and it had 3.36 A of d_{002}, *ca.* 170 A of Lc. It was 12 μm in diameter with an average length of 50 μm. A fully-oriented lamella structure of crystal domain was shown by the analyses of XRD patterns (Phillips PW 1830) and SEM photographs (Hitachi S-2700), respectively.

Electrode Preparation. The MPCF electrode was prepared as a 60 μm thick, 10 cm × 4.15 cm sheet on one side of a piece of copper foil (12 μm) by coating with the slurry, drying at 110 °C and pressing. The slurry was a mixture of MPCF, polyvinylidene fluoride (PVdF) and 1-methylpyrrolidone (NMP) (weight ratio; 90 : 10 : 100). The counter electrode was prepared as a 150 μm sheet on one side of a 13 cm × 4.0 cm piece of aluminum foil (25 μm) by a process similar to that of the MPCF electrode. The counter electrode slurry was a mixture of $LiCoO_2$ (FMC Ltd.), super S black, PVDF and NMP (weight ratio; 92 : 3 : 5 : 100). Lithium metal was used as a reference electrode.

Cell Assembly. Laminates of the MPCF electrode, $LiCoO_2$ electrode and separator (Celgard 2500) were wound into the so-called jelly roll by a winding machine (Adlin model of Automation Co.). Three electrode test cells consisted of a Pyrex glass tube containing the jelly roll with the lithium reference and an electrolytic solution of 1M $LiPF_6$ in ethylene carbonate and diethyl carbonate (1 : 1) (Merck). The assembly process is illustrated in Scheme 1.

Electrochemical Test. The assembled cell was tested by galvanostatic charge-discharge by the Maccor series 2000 charge-discharge tester. The cut-off potential limits of the MPCF electrode was 20 mV_{Li/Li^+} for charging and 1500 mV_{Li/Li^+} for discharging versus the lithium reference electrode. Current density was 26.0 mA/g-MPCF. To evaluate the initial capacity fading characteristics, three tests were performed before the normal galvanostatic charge-discharge. Detailed test conditions are described in the corresponding figures.

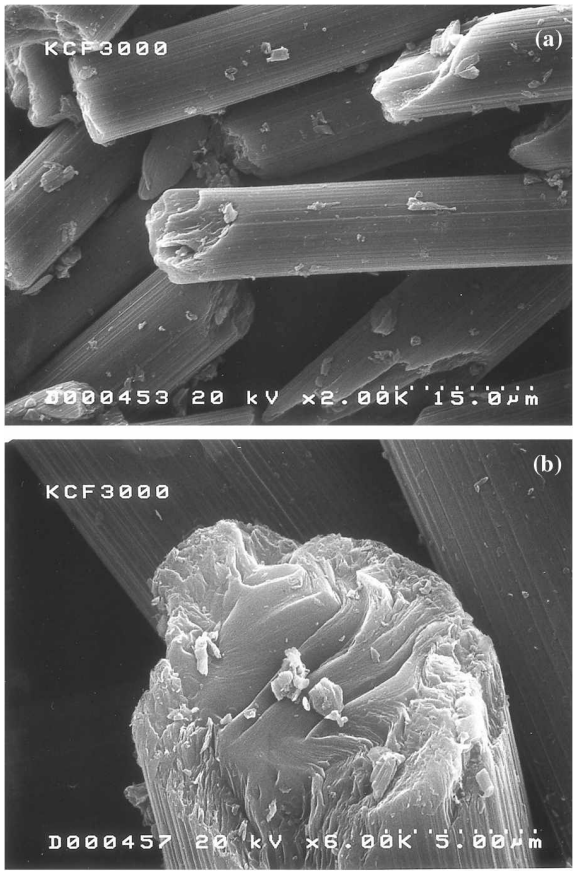

Figure 1. SEM images of pristine MPCF3000. (a) longitudinal view (b) cross-sectional view

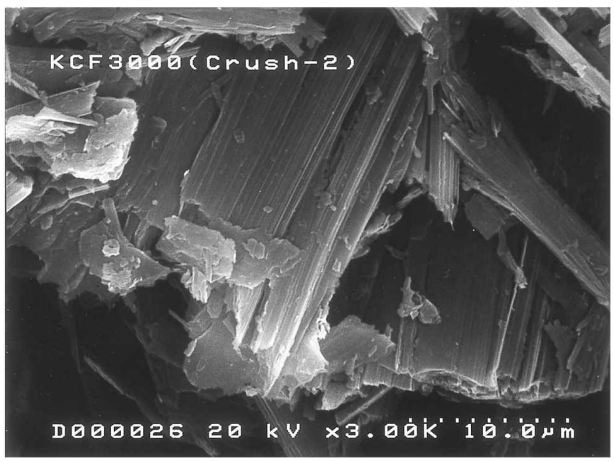

Figure 2. SEM image of crushed MPCF3000.

Results and Discussion

Surface electron microscopy images of MPCF as it was received, referred to as pristine, are shown in Figure 1a for the longitudinal view and Figure 1b for the cross-sectional view. The cross-sectional view shows that the crystal structure varies between the surface and internal area of the fiber. When MPCF was milled by attrition with zirconia balls, the fiber was split into a firewood shape, refferred to as the crushed sample, as shown in Figure 2.

The difference between pristine and crushed MPCF was analysed by x-ray diffraction using carbonxs[21] program simulation. The XRD pattern of pristine and crushed MPCF is shown in Figure 3 and Figure 4, respectively. Carbonxs simulated data from obtained XRD data are also presented together with measured data, with good correspondence. The crystal structural properties of the internal moiety of the fiber could be presented a little more clearly by XRD data of the crushed sample compared with the pristine sample because the XRD pattern of the former was taken from the

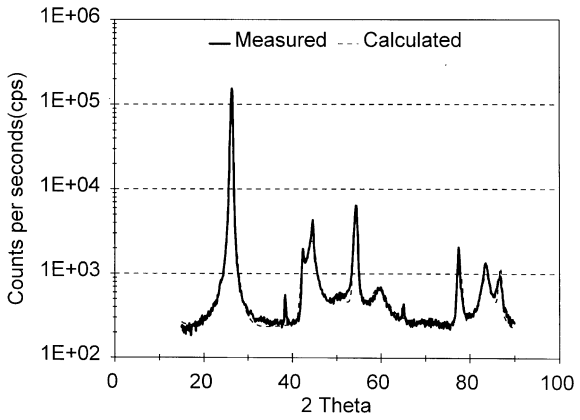

Figure 3. XRD pattern of pristine MPCF3000 with carbonxs data simulation.

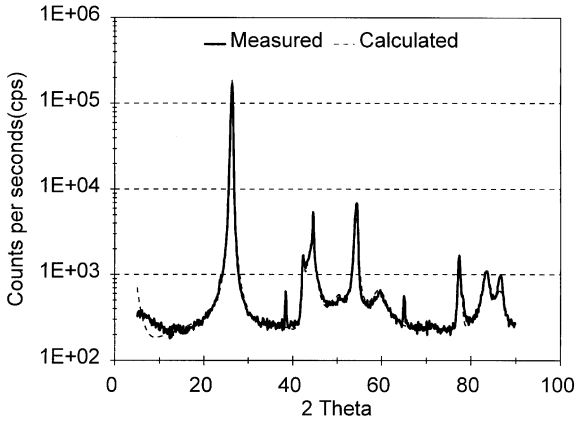

Figure 4. XRD pattern of crushed MPCF3000 with carbonxs data simulation.

enhanced portion of internal moiety from split fiber. The crystal structural parameters from XRD data simulation are listed in Table 1. Compared with the pristine sample, the crushed sample has low probability of random stacking (Pr), high La (coherence length in the AB plane) and high M (total number of layers). This means that the crushed sample has better crystal structure than the pristine sample. Also, the internal area of the fiber has a higher graphitic structure than the fiber surface. In view of the electrochemical characteristics, the surface and internal areas have carbon and graphite-like properties, respectively.

An electrochemical test was performed using the pristine sample only. The prepared electrode did not include crushed MPCF as presented in the SEM image in Figure 5.

Figure 6 and Figure 7 show a potential profile and a differential-capacity of the MPCF electrode at the first cycle with a specific current of 26 mA/g-MPCF and a potential range of 20-1500 mV_{Li/Li^+}. Overall, the pattern has the general behavior of artificial graphite. But, the potential plateau around 37 mV_{Li/Li^+} during charge was observed, which is absent in the case of natural graphite. Our work focused on the behavior of this potential plateau. Figure 8, Figure 9 and Figure 10 show potential variations and the differential potentiogram, and the specific capacities and Ah efficiencies by charge-discharge cycle number during charge-discharge processes.

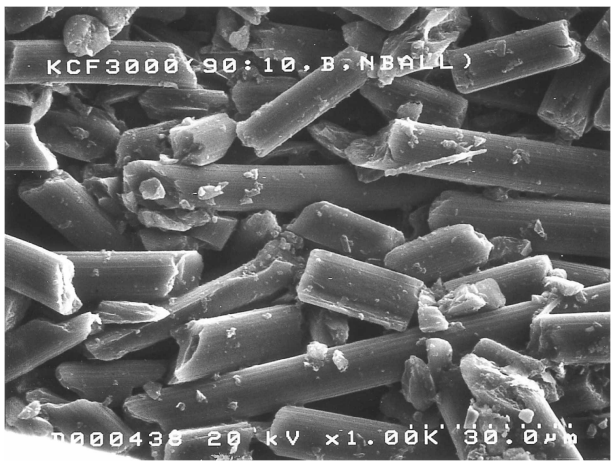

Figure 5. SEM image of MPCF3000 electrode.

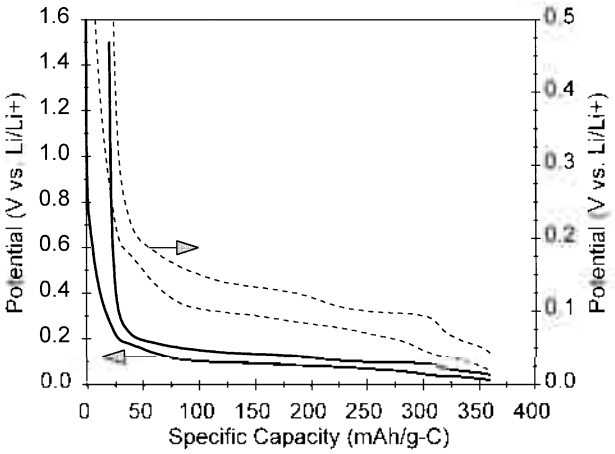

Figure 6. Potential profile of MPCF3000/1M $LiPF_6$/EC+DEC (1 : 1)/Li cell at the first cycle.

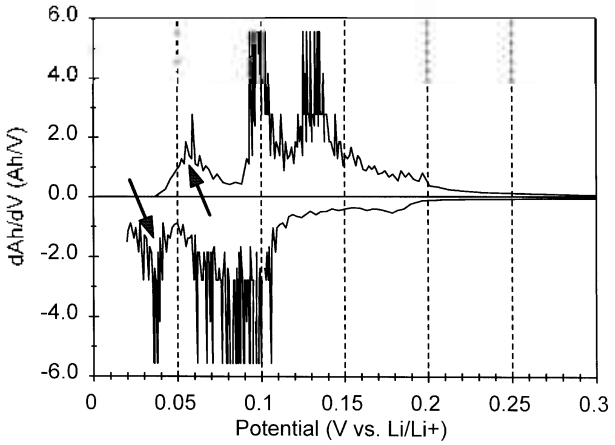

Figure 7. Differential-capacity profile of MPCF3000/1M $LiPF_6$/EC+DEC (1 : 1)/Li cell at the first cycle.

For the first cycle, the specific capacity and Ah efficiency were 341 mAh/g-C and 95%, respectively, for the conditions of a current density of 26 mA/g-carbon and a potential range of 20-1500 mV_{Li/Li^+}. At the tenth cycle, the specific capacities to 80 mV_{Li/Li^+} fell were rapidly, reaching 23% of the first cycle's value (48 mAh/g-MPCF). But, the specific capacity

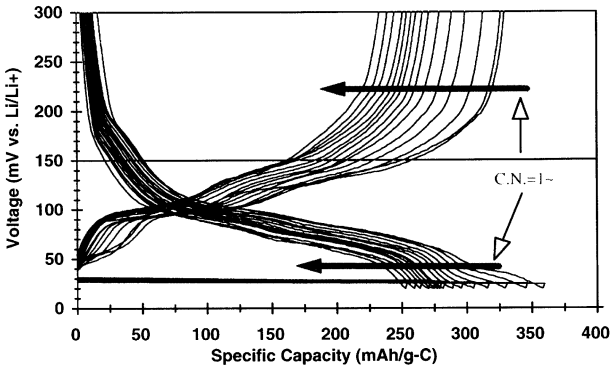

Figure 8. Variation of potential profile of MPCF3000/1M $LiPF_6$/EC+DEC (1 : 1)/Li cell by the charge/discharge cycling.

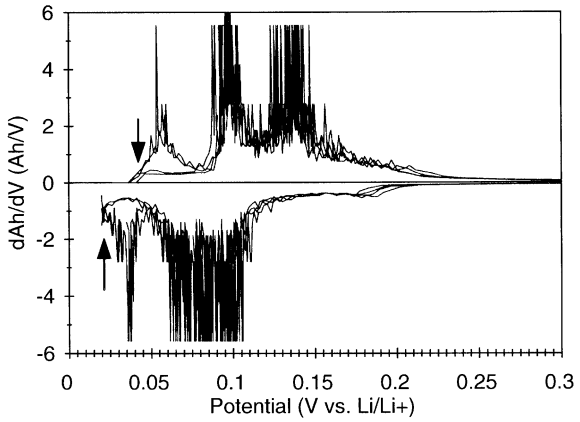

Figure 9. Differential-capacity profile of MPCF3000/1M $LiPF_6$/EC+DEC (1 : 1)/Li cell of 1st, 2nd and 10th charge/discharge cycling.

between 80 mV_{Li/Li^+} and 1500 mV_{Li/Li^+} fell slowly, as presented in Figure 8 and Figure 9. This capacity fading pattern is also described in Figure 10 to show the gradual degradation of the potential plateau at *ca.* 50 mV_{Li/Li^+} during discharge. Therefore, the overall specific capacities fell with cycling, fast fading to the seventh cycle and loose fading from the seventh cycle. In Table 2, capacity fading and Ah

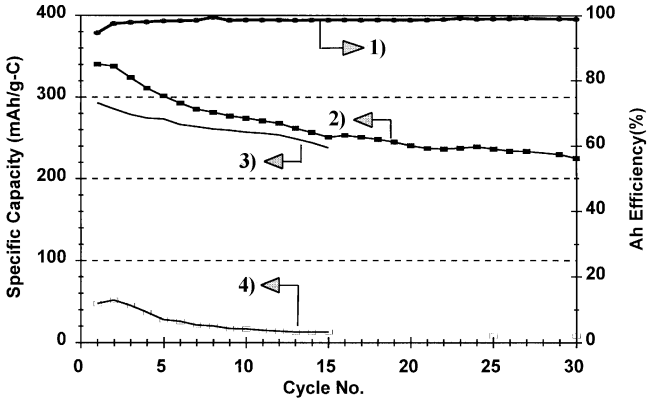

Figure 10. Variations of specific capacities and Ah efficiencies with charge/discharge cycling based on Fig. 8. 1) Ah efficiency. 2) total specific capacity (20-1500 mV_{Li/Li^+}). 3) specific capacity of 80-1500 mV_{Li/Li^+}. 4) specific capacity of 20-80 mV_{Li/Li^+}

Table 1. Crystal Structural Parameters by the Simulation of XRD Data

pristine	crushed	Parameters
2.4523	2.4570	A, In plane cell constant (Å)
3.3576	3.3619	d_{002}, Interlayer spacing (Å)
59.62	174	La, Coherence length in the AB plane (A)
50.29	756	M, Total number of layers
0.284	0.272	Pr, Probability of random stacking
0.025	0.027	Pt, Probability of 3R stacking

Table 2. Capacity Fading and Ah Efficiencies According to Potential Region

Properties	Cycle No.	Potential Region (mV_{Li/Li^+})		
		20~1500	20~80	80~1500
Specific Capacity (mAh/g-MPCF)	1	341	48	293
	7	286	22	264
Reducing Rate		16%	54%	10%
Ah Efficiency (%)	1	94.7	74.1	99.2
	7	98.6	81.4	100.2
Increment of Ah eff.		3.9%	7.3%	1%

efficiencies according to the potential region, are summarized. The fast capacity fading until the seventh cycle is due to the gradual fading of reversibility of the plateau region at around the potential of 37 mV_{Li/Li^+}. This gradual fading of reversibility might be linked to the trapping of lithium within the carbon structure. This gradual capacity fading leads to low Ah efficiencies from the second cycle to about the tenth cycle compared with high Ah efficiencies after the eleventh cycle. Therefore, the origin of initial capacity fading is due to the fading of the reversibility of the plateau region at around 37 mV_{Li/Li^+}.

Three different tests were applied to the MPCF electrode to evaluate the capacity fading characteristics of the potential plateau at around 37 mV_{Li/Li^+}.

First, we changed the charge limit potential of the electrode. With a specific current of 23.6 mA/g-MPCF, the MPCF electrode was charged to 50 mV_{Li/Li^+}, and then discharged to 1500 mV_{Li/Li^+} from the first through tenth cycle. From the eleventh cycle, the charge potential limit was changed to 5 mV_{Li/Li^+}. Test results are shown in Figure 11 and Figure 12. At the charge limit potential of 50 mV_{Li/Li^+}, good cycling performance was obtained. But at the charge limit potential of 5 mV_{Li/Li^+}, the specific capacity fell gradually due to the capacity fading at about the 37 mV_{Li/Li^+} region (see 4) in Figure 12).

The 37 mV_{Li/Li^+} region's capacity for the MPCF electrode is completely deminished by a one-time full charge, as shown in Figure 13. The first charge was achieved by constant current step cycling of 20 times to 5 mV_{Li/Li^+} by the specific current of 22.7 mA/g-MPCF with 30 minutes rest time between each step and then 20 times cycling to 5 mV_{Li/Li^+} by the specific current of 3.78 mA/g-MPCF with 30 minutes step-to-step rest time. Then, normal constant current

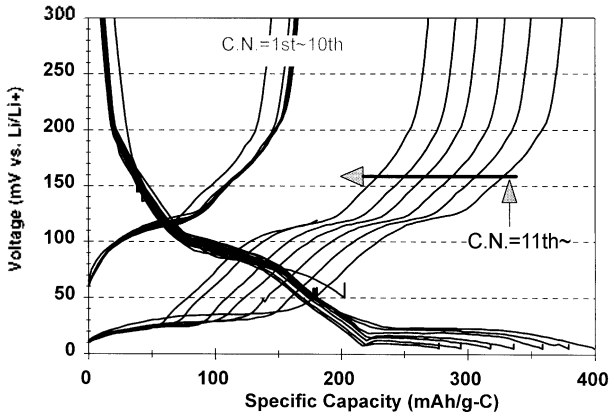

Figure 11. Variation of potential profile of MPCF3000/1M $LiPF_6$/EC+DEC (1 : 1)/Li cell with potential range of 50-1500 mV_{Li/Li^+} from the 1st to 10th cycles and then 5-1500 mV_{Li/Li^+} from 11th cycle

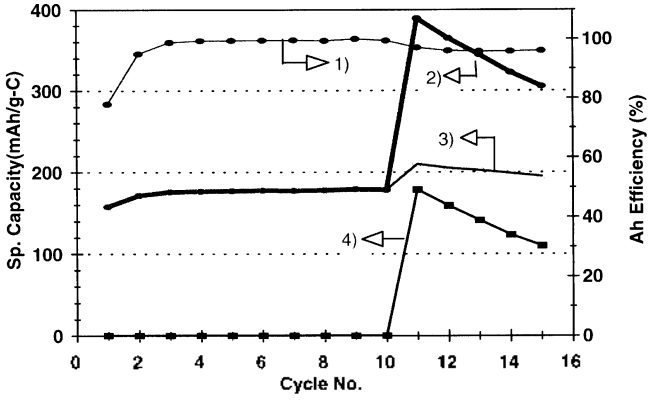

Figure 12. Variations of specific capacities and Ah efficiencies with charge/discharge cycling based on Fig. 11. 1) Ah efficiency. 2) total specific capacity (5-1500 mV_{Li/Li^+}). 3) specific capacity of 50-1500 mV_{Li/Li^+}. 4) specific capacity of 5-50 mV_{Li/Li^+}

cycling was performed between potential the limits of 5 mV_{Li/Li^+} and 1500 mV_{Li/Li^+} for charge and discharge, respectively, by the specific current of 22.7 mA/g-MPCF300.

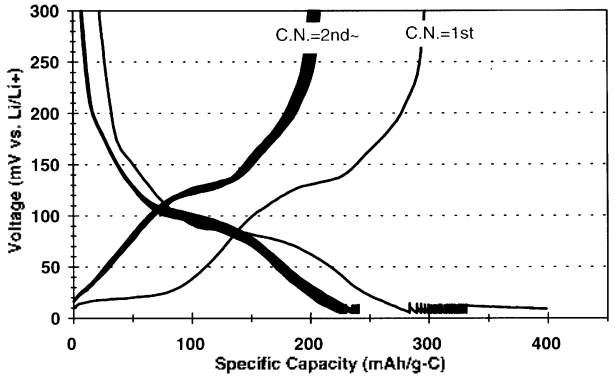

Figure 13. Variation of potential profile of MPCF3000/1M $LiPF_6$/EC+DEC (1 : 1)/Li cell with current step cycling of the 1st charge to 5 mV_{Li/Li^+} and 30 minutes for 20 cycling with 22.7 mA/g and then another 20 cycling with 3.78 mA/g of specific current. after then normal cycling of potential range of 5-1500 mV_{Li/Li^+} with 22.7 mA/g from the 1st discharge.

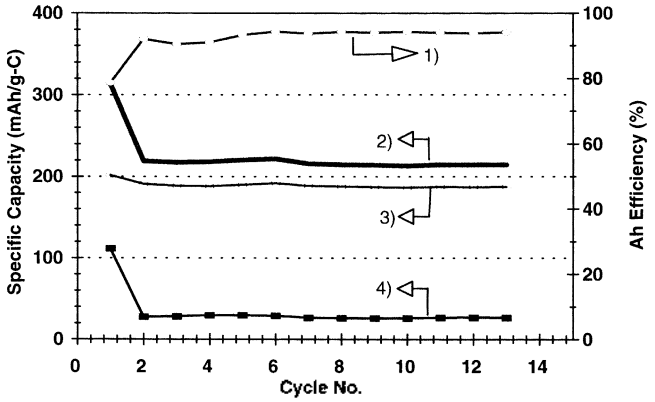

Figure 14. Variations of specific capacities and Ah efficiencies with charge/discharge cycling based on Fig. 13. 1) Ah efficiency. 2) total specific capacity (5-1500 mV_{Li/Li^+}). 3) specific capacity of 50-1500 mV_{Li/Li^+}. 4) specific capacity of 5-50 mV_{Li/Li^+}

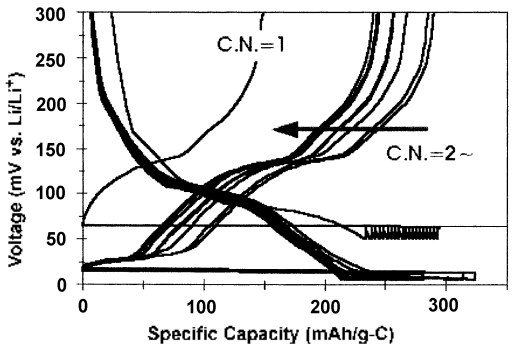

Figure 15. Variation of potential profile of MPCF3000/1M $LiPF_6$/EC+DEC (1 : 1)/Li cell with current step cycling of the 1st charge to 50 mV_{Li/Li^+} and 30 minutes for 20 cycling with 22.7 mA/g, after then normal cycling of potential range of 5-1500 mV_{Li/Li^+} with 22.7 mA/g from the 1st discharge.

Results are presented in Figure 13 and Figure 14. At less than 50 mV_{Li/Li^+} for first charge, *ca.* 184 mAh/g of specific capacity can be charged, but only 110 mAh/g of specific capacity can be discharged, leading to the irreversible specific capacity of 74 mAh/g. From the second normal cycling, the specific capacity at less than 50 mV_{Li/Li^+} was stabilized to

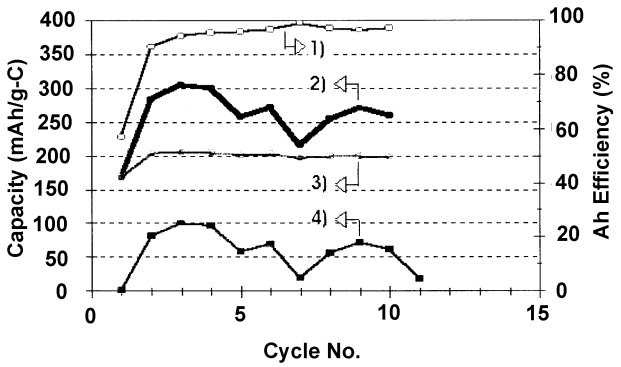

Figure 16. Variations of specific capacities and Ah efficiencies with charge/discharge cycling based on Fig. 15. 1) Ah efficiency. 2) total specific capacity (5-1500 mV_{Li/Li^+}). 3) specific capacity of 50-1500 mV_{Li/Li^+}. 4) specific capacity of 5-50 mV_{Li/Li^+}

about 30 mAh/g without a potential plateau less than 50 mV_{Li/Li^+}.

An experiment similar to the above was performed with a charge limit potential of 50 mV_{Li/Li^+}, as presented in Figure 15 and Figure 16. Full charge to 50 mV_{Li/Li^+} has minimal effect on the 37 mV_{Li/Li^+} region's potential plateau. Therfore, during normal cycling, the behavior of the potential plateau of the 37 mV_{Li/Li^+} region shows the same pattern as in Figure 8, Figure 9, and Figure 10.

Conclusion

Based on our results, we can conclude the following: 1) The reversible potential plateau was observed at a potential region of 30-60 mV_{Li/Li^+}. 2) This potential plateau disappeared with cycling, therefore, fast capacity fading and low Ah efficiency were observed. 3) This potential plateau was not affected by charging to 50 mV_{Li/Li^+}. When the electrode was charged by a constant current step pulse to the potential of 5 mV_{Li/Li^+}, the plateau appeared only within the first cycle. 4) Finally, the origin of the initial capacity fading might be due to the result of lithium ion trapping within the MPCF structure.

Acknowledgment. This work is part of the Mid-term Technology project supported by the Ministry of Commerce, Industry and Energy of Korea.

References

1. Sleigh, A. K.; Saken, U. von *Solid State Ionics* **1992**, *57*, 90.
2. Dahn, J. R.; Sleigh, A. K.; Shi, H.; Reimers, J. N.; Zhong, Q.; Way, B. M. *Electrochemica Acta* **1993**, *38*, 1179.
3. Fischbach, D. B. In *Chemistry and Physics of Carbon*; Walker, Jr. P. L., Ed.; Marcel Dekker Inc.: New York, 1971; Vol. 7, p 1.
4. Shi, H. *Ph.D. Thesis*; Simon Fraser University: 1993.
5. Dahn, J. R.; Fong, R.; Spoon, M. J. *Phy. Rev. B* **1990**, *42*, 6424.
6. Shu, Z. X.; McMillan, R. S.; Murray, J. J. *J. Electrochem. Soc.* **1993**, *140*, 922.
7. Dahn, J. R. *Phy. Rev. B* **1991**, *44*, 9170.
8. Guerard, D.; Herold, A. *Carbon* **1975**, *13*, 337.
9. Mabuchi, A.; Fujimoto, H.; Tokumitsu, K.; Kasuh, T. *J. Electrochem. Soc.* **1995**, *142*, 3049.
10. Mabuchi, A.; Tokumitsu, K.; Fujimoto, H.; Kasuh, T. *J. Electrochem. Soc.* **1995**, *142*, 1041.
11. Winter, M.; Novak, P.; Monnier, A. *J. Electrochem. Soc.* **1998**, *145*, 428.
12. Zheng, T.; McKinnon, W. R.; Dahn, J. R. *J. Electrochem. Soc.* **1996**, *143*, 2137.
13. Peled, E.; Eshkenaz, V.; Rosenberg, Y. *J. Power Sources* **1998**, *76*, 153.
14. Takami, N.; Satoh, A.; Ohsaki, T.; Kanda, M. *J. Electrochem. Soc.* **1998**, *145*, 478.
15. Mori, Y.; Iriyama, T.; Hashimoto, T.; Yamazaki, S.; Kawakami, F.; Shiroki, H. *J. Power Sources* **1995**, *56*, 205.
16. Yamabe, T.; Tanaka, K.; Ago, H.; Yoshizawa, K.; Yata, S. *Synthetic Metals* **1997**, *86*, 2411.
17. Hankinson, D. J.; Almlof, J. *J. Mol. Structure* **1996**, *388*, 245.
18. Komoda, S.; Watanabe, M.; Komada, S.; Osaka, T.; Kikuyama, S.; Yuasa, K. *Electrochemica Acta* **1998**, *43*, 3127.
19. Tatsumi, K.; Zaghib, K.; Sawada, Y. *J. Electrochem. Soc.* **1995**, *142*, 1090.
20. Tatsumi, K.; Satoh, A.; Hara, M.; Ohasaki, T. *J. Electrochem. Soc.* **1995**, *142*, 371.
21. Shi, H.; Reimers, J. M.; Dahn, J. R. *J. Appl. Cryst.* **1993**, *26*, 827.